The new magnetic Doppler imaging code

N. Piskunov

Uppsala Astronomical Observatory, Box 515, SE-751 20 Uppsala, Sweden

Abstract. In this paper we describe a new Magnetic Doppler Imaging (MDI) code **INVERS10** designed to reconstruct magnetic fields on the surfaces of CP stars. The code is based on a state-of-the-art radiative transfer solver and efficient minimization technique. It is aimed at multi-processor calculations. This new tool is capable of reconstructing the distribution of magnetic field vectors and abundance of one chemical element from a time sequence of four Stokes parameters, observed with sufficient time and spectral resolution. No assumptions about field geometry (e.g. multipolar, radial etc.) are necessary. In addition, **INVERS10** is capable of simulating the observed profiles for a given field geometry and abundance distribution. We also show some results of numerical experiments and discuss future applications of the new code.

1. Introduction

The study of stellar magnetic fields plays a very important role in our understanding of star formation and evolution linking the photosphere to stellar interiors and to the circumstellar medium. The reliable determination of field geometries for a statistically significant number of objects will serve as a crucial test for existing and future stellar models.

The technique of detection of magnetic fields is quickly maturing. Both broad-band linear polarimetry and spectropolarimetry have been perfected to a level where polarization of 10^{-4} can be reliably measured. Modeling the field even for larger polarization levels requires a major effort. One promising technique is Doppler Imaging (DI). DI has been originally suggested (Deutsch, **1958)** and developed (e.g. Goncharsky et al., **1982)** for mapping chemical elements on chemically peculiar stars. The method allows extraction of information out of the rotational modulation of spectral line profiles. DI has been successfully extended to multi-element mapping, to late-type stars, eclipsing binary systems etc. Modeling the magnetic field is considerably more demanding: the observations are influenced not only by the field strength, but also by orientation which changes as the star rotates. Our new MDI code is capable of mapping the field vector and one additional scalar parameter. It was logical to apply this code first to magnetic CP stars where, on one hand, the fields are strong and globally organized and, on the other hand, a wealth of observational data already exists.

In the following sections we describe the solution of the radiative transfer for four Stokes parameters, the optimization procedure, the structure of **INVERS10** and the implementation of the parallel calculations. Next we show the results of numerical experiments that demonstrate the performance of the new code and help in establishing the requirements to the observations.

2. Synthesis of stellar spectra

The core of any Magnetic Doppler Imaging code is the radiative transfer solver (RTS) which must be sufficiently accurate to represent the wavelength-dependent Stokes parameters radiated from each element on the stellar disk and fast enough because that is where MDI spends most of its computing time.

The equation of radiative transfer in the magnetic case is a system of 4 ordinary differential equations for the Stokes vector $\boldsymbol{I} = \{I, Q, U, V\}$:

$$\frac{d\boldsymbol{I}}{dz} = -\mathcal{K}\boldsymbol{I} + \boldsymbol{J}, \tag{1}$$

where the absorption matrix $\mathcal{K}$ and emission vector $\boldsymbol{J}$ are given by:

$$\mathcal{K} = k_c \mathbb{1} + \sum_{\text{lines}} k_0^{\text{line}} \Phi_{\text{line}}, \tag{2}$$

$$\boldsymbol{J} = k_c S_c e_0 + \sum_{\text{lines}} k_0^{\text{line}} S_{\text{line}} \Phi_{\text{line}} e_o. \tag{3}$$

Here $\mathbb{1}$ is the identity 4x4 matrix, $e_0 = \{1,0,0,0\}^t$, and k_c and S_c are the continuum opacity and source function. The line opacity consists of a sum over all contributing lines of the absorption matrices Φ times the line center opacity k_0^{line}. We assume an unpolarized continuum and LTE throughout the rest of the paper. The polarization of the continuum is irrelevant for an MDI code, it contains little information about surface structures and is small compared to the magnetic polarization in spectral lines. The NLTE effects

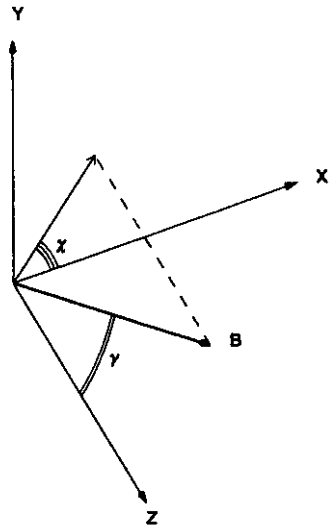

Figure 1: *The orientation of the magnetic field vector in the observer reference frame (Z is the line of sight) is defined by the angles γ and χ. γ is measured between the direction to the observer and the direction of the field vector: $\gamma \in [0°, 180°]$. χ is measured in the image plane from the X-axis counter-clockwise.*

are more difficult to include when dealing with complex blends (although there are several NLTE RTS codes for non-magnetic and even magnetic cases), but here we prefer to restrict ourselves to lines formed in LTE which allows us to write the emission vector as:

$$J = k_c \mathrm{B}_\lambda(T) e_0 + \mathrm{B}_\lambda(T) \sum_{\text{lines}} k_0^{\text{line}} \Phi_{\text{line}} e_o. \tag{4}$$

Finally we can write the expressions for the absorption matrix Φ:

$$\Phi = \begin{pmatrix} \phi_I & \phi_Q & \phi_U & \phi_V \\ \phi_Q & \phi_I & \psi_V & -\psi_U \\ \phi_U & -\psi_V & \phi_I & \psi_Q \\ \phi_V & \psi_U & -\psi_Q & \phi_I \end{pmatrix}, \tag{5}$$

where:

$$\begin{aligned} \phi_I &= 1/2(\phi_p \sin^2\gamma + 1/2(\phi_r + \phi_b)(1 + \cos^2\gamma)) \\ \phi_Q &= 1/2(\phi_p - 1/2(\phi_r + \phi_b)) \sin^2\gamma \cos 2\chi \\ \phi_U &= 1/2(\phi_p - 1/2(\phi_r + \phi_b)) \sin^2\gamma \sin 2\chi \\ \phi_V &= 1/2(\phi_r - \phi_b) \cos\gamma \\ \psi_Q &= 1/2(\psi_p - 1/2(\psi_r + \psi_b)) \sin^2\gamma \cos 2\chi \\ \psi_U &= 1/2(\psi_p - 1/2(\psi_r + \psi_b)) \sin^2\gamma \sin 2\chi \\ \psi_V &= 1/2(\psi_r - \psi_b) \cos\gamma. \end{aligned} \tag{6}$$

The angles determine the orientation of the field vector in the observer reference frame as shown in Figure 1. The ϕ's and the ψ's in absorption matrix (5) describe the absorption and anomalous dispersion profiles. For a given transition with magnetic quantum numbers of Zeeman states $\mathbf{M}_{\text{lower}}$ and $\mathbf{M}_{\text{upper}}$ we denote the type of transition allowed by the selection rule as:

$$\Delta M = M_{\text{upper}} - M_{\text{lower}} = \left\{ \begin{array}{ccc} +1 & \equiv & b \\ 0 & \equiv & p \\ -1 & \equiv & r \end{array} \right\}. \tag{7}$$

In a moderate magnetic field (< 10^6 Gauss) and assuming LS coupling, a level with quantum numbers *L*, *S* and ***J*** splits into $2\boldsymbol{J}+1$ states with $\boldsymbol{M}$ = -J,...., 0,...., +***J*** with Lande factors:

$$g = \frac{3}{2} + \frac{S(S+1) - L(L+1)}{2J(J+1)}. \tag{8}$$

For a permitted transition between two Zeeman states the wavelength shift relative to the line center at a zero field is:

$$\Delta\lambda = \frac{e\lambda_0^2 |\vec{\mathrm{B}}|}{4\pi m c^2} \left(g_{\text{lower}} M_{\text{lower}} - g_{\text{upper}} M_{\text{upper}}\right). \tag{9}$$

For similar Lande factors of upper and lower levels a red shift corresponds to a negative ΔM which explains the convention introduced in (7).
The absorption profiles:

$$\begin{aligned} \phi_b &= \sum_b A_b H(a, v - \Delta\lambda_b/\Delta\lambda_{\text{Dop}}) \\ \phi_p &= \sum_p A_p H(a, v - \Delta\lambda_p/\Delta\lambda_{\text{Dop}}) \\ \phi_r &= \sum_r A_r H(a, v - \Delta\lambda_r/\Delta\lambda_{\text{Dop}}) \end{aligned} \tag{10}$$

and the anomalous dispersion profiles:

$$\begin{aligned} \psi_b &= 2\sum_b A_b F(a, v - \Delta\lambda_b/\Delta\lambda_{\text{Dop}}) \\ \psi_p &= 2\sum_p A_p F(a, v - \Delta\lambda_p/\Delta\lambda_{\text{Dop}}) \\ \psi_r &= 2\sum_r A_r F(a, v - \Delta\lambda_r/\Delta\lambda_{\text{Dop}}) \end{aligned} \tag{11}$$

are well described (in most cases) by the Voigt and Faradey-Voigt functions:

$$H(a,v) = \frac{a}{\pi} \int_{-\infty}^{+\infty} \frac{exp(-y^2)}{(v-y)^2 + a^2} dy, \tag{12}$$

$$F(a,v) = \frac{1}{2\pi} \int_{-\infty}^{+\infty} \frac{(v-y) exp(-y^2)}{(v-y)^2 + a^2} dy. \tag{13}$$

Humlic'ek (1982) provides a fast and accurate approximation for both functions (note that the imaginary part of his approximation corresponds to 2*F*, rather than *F*). The normalization of individual Zeeman components is done separately for *b*, ***p*** and *r* so that: $\sum A_b = \sum A_p = \sum A_r = 1$. The Voigt ***a*** and ***v*** are the Lorentzian line width and the offset from the

line center expressed in units of Doppler width:

$$a = \frac{\Gamma_{\rm Rad} + \Gamma_{\rm Stark} + \Gamma_{vanderWaals}}{4\pi\Delta\nu_{\rm Dop}} \quad (14)$$

$$v = (\lambda - \lambda_0)/\Delta\lambda_{\rm Dop}. \quad (15)$$

In order to solve the RT equation (1) for a given location on the stellar surface we need to:

- compute the Voigt a and v from equations (14) and (15),
- compute Voigt and Faradey-Voigt functions for each Stokes component,
- compute ϕ's and ψ's using equations (10-11),
- compute the continuous opacity coefficient,
- compute the absorption matrix Φ from equation (5) for each contributing spectral line and add them together to form the absorption matrix $\mathcal{K}$ and the emission vector J throughout the atmosphere.

We will not discuss here the calculations of damping parameters, in the case where they are not directly available from a line database like, e.g. VALD (Piskunov et al., 1995), or the calculations of different continuous opacities because INVERS10 inherited these parts from our non-magnetic spectral synthesis code SYNTH (Piskunov, 1992).

Once the absorption matrix and the emission vector are prepared, we are ready to solve the equation of radiative transfer (1). The first code, capable of doing this job, was created by Landi DegPInnocenti (1976), but the Runge-Kutta integrator used there is too slow for our purpose. Instead we have considered two types of more effcient RTS for INVERS10: Feautrier and Diagonal Element Lambda Operator (DELO).

2.1. Feautrier RTS

The Feautrier method is well established as the most stable and fast long characteristics RTS for the non-magnetic case. Therefore, it was logical to extend it to the case of magnetic field. Such an algorithm was first formulated by Auer et al. (1977) (AHH). Here we repeat the basic formulae from the seminal AHH paper to help comparing different RTS.

As in the conventional (non-magnetic) case, the intensity is split into two flows: I^+ for radiation propagating towards the surface and I^- for radiation directed inside the star. Next after introducing the two new variables $P = (I^+ + I^-)/2$ and $R = (I^+ - I^-)/2$ the equation of radiative transfer is replaced by a second-order differential equation for P.

The same principle is generalized to the magnetic case as follows. Let I^+ be the Stokes vector characterizing the radiation propagating out of the atmosphere while I^- corresponds to the radiation in the opposite direction. Note that for I^- we also have to switch the b and the r Stokes components as the wavelength

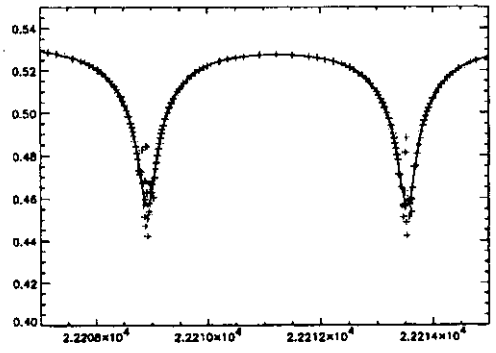

Figure 2: ***The effects of numerical instability caused by an ill-conditioned opacity matrix $\mathcal{K}$ in the longitudinal field for the infrared Ti I 22211.228 Å line with Landé factor 2.08. The plot represents disk center intensity (in arbitrary units) as a function of wavelength for $T_{\rm eff}$=3500 K, $\log g$=5 model of Allard and Hauschildt (1995) with a radial field of 4 kG. Plus signs show the results of calculations based on direct matrix inversion, while the spectrum computed by solving systems of linear equations is shown with a solid line.***

shifts will change signs. The switch of direction corresponds to the change of angles to 180° - γ and to $-\chi$. Therefore, the line absorption matrix for I^+ is related to the matrix for I^- as:

$$\Phi^+ = \begin{pmatrix} \phi_I^+ & \phi_Q^+ & \phi_U^+ & \phi_V^+ \\ \phi_Q^+ & \phi_I^+ & \psi_V^+ & -\psi_U^+ \\ \phi_U^+ & -\psi_V^+ & \phi_I^+ & \psi_Q^+ \\ \phi_V^+ & \psi_U^+ & -\psi_Q^+ & \phi_I^+ \end{pmatrix} = \begin{pmatrix} \phi_I^- & \phi_Q^- & -\phi_U^- & \phi_V^- \\ \phi_Q^- & \phi_I^- & -\psi_V^- & -\psi_U^- \\ -\phi_U^- & \psi_V^- & \phi_I^- & -\psi_Q^- \\ \phi_V^- & \psi_U^- & \psi_Q^- & \phi_I^- \end{pmatrix} = \Phi^-. \quad (16)$$

This follows from equations (5) and (6) and from the fact that the Voigt function (eq. 12) is symmetric and the Faradey-Voigt function (eq. 13) is anti-symmetric, leading to an additional sign change for all ψ^- but not for ϕ^-. One can clearly see that Φ^- can be made identical to Φ^+ if we define I^- as $\{I, Q, -U, V\}^{\rm t}$. For the new definition of the radiation flows we can write two identical radiative transfer equations:

$$\pm\frac{dI^\pm}{dz} = -\mathcal{K}I^\pm + J, \quad (17)$$

and after adding and subtracting them and introducing the Feautrier variables $P = (I^+ + I^-)/2$ and $R = (I^+ - I^-)/2$ we get the familiar equations:

$$\frac{dP}{dz} = -\mathcal{K}R, \quad (18)$$

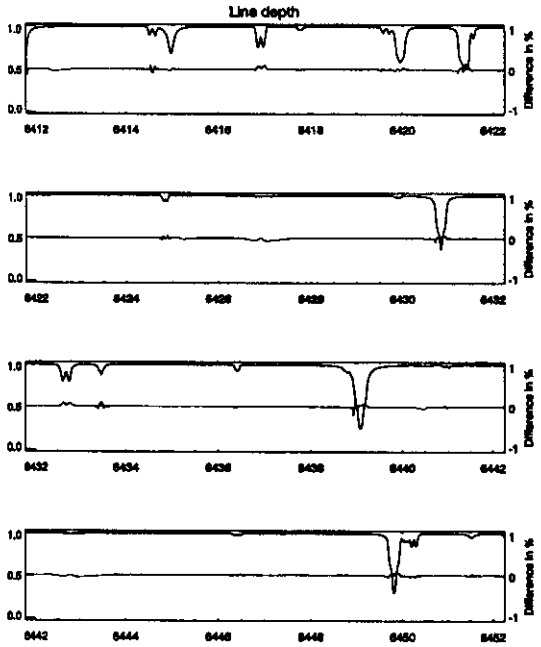

Figure 3: *The comparison of the intensity spectra computed with Feautrier and DELO solvers for the center of the Sun. The magnetic field was assumed to be radial with* $|\vec{B}| = 2\,kG$. *The line in the middle of each panel gives the relative difference between the two spectra (DELO – Feautrier).*

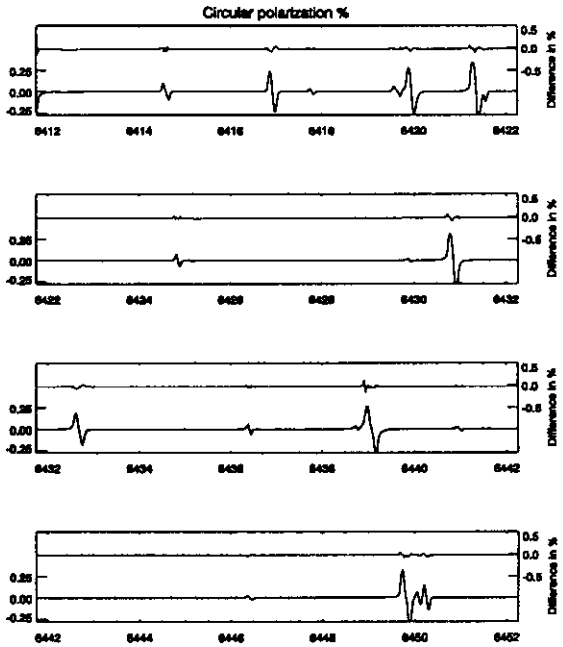

Figure 4: *The comparison of the V Stokes spectra computed with Feautrier and DELO solvers for the center of the Sun. The magnetic field was assumed to be radial with* $|\vec{B}| = 2\,kG$. *The upper line in each panel gives the relative difference between the two spectra (DELO – Feautrier).*

$$\frac{dR}{dz} = -\mathcal{K}P + J. \tag{19}$$

We combine them to a single 2nd-order equation for P:

$$\frac{d}{dz}\left(\mathcal{K}^{-1}\frac{dP}{dz}\right) = \mathcal{K}P + J. \tag{20}$$

Boundary counditions are set on both ends of the integration path:

$$\mathcal{K}^{-1}\frac{dP}{dz} = -P \qquad \text{at the surface,} \tag{21}$$

$$\mathcal{K}^{-1}\frac{dP}{dz} = P - I^{+} \qquad \text{at maximum } z. \tag{22}$$

We follow AHH in using the Taylor expansion to improve the approximation at the inner boundary:

$$I^{+} = \left(B_\lambda - \mathcal{K}^{-1}\frac{dB_\lambda}{dz}\right) e_0. \tag{23}$$

At this point, we note that we can easily switch from the simple geometrical depth scale along the line of sight z to the depth scale perpendicular to the surface z' by introducing μ - the cosine of the angle between z and z'. Furthermore, model atmospheres (e.g. Kurucz grid (1993) are often computed on a scale of column mass rather than geometrical depth. We can switch to this scale by replacing k^c and k_0^{line} computed per unit of length, with opacities computed per unit of mass and introducing elementary mass increment: $dm \equiv \rho dz'$ (ρ is density).

$$\begin{aligned} \mu^2\frac{d}{dm}\left(\mathcal{K}^{-1}\frac{dP}{dm}\right) &= \mathcal{K}P + J \\ \mathcal{K}^{-1}\frac{dP}{dm} &= -P|_{m_0} \\ \mathcal{K}^{-1}\frac{dP}{dm} &= P - e_0\left(B_\lambda - \mathcal{K}^{-1}\frac{dB_\lambda}{dm}\right)\Big|_{m_N}. \end{aligned} \tag{24}$$

On a discrete grid equations (24) can be represented with finite differences. For depth points i=0, 1,...., N - 1 we define the quantities:

$$\delta_i = m_i - m_{i+1} \text{ and } \Delta_i = \left(\mathcal{K}_{i+1}^{-1} + \mathcal{K}_i^{-1}\right)/2\delta_i. \tag{25}$$

Then the Feautrier scheme becomes equivalent to a

system of linear equations:

$$\begin{pmatrix} \mathcal{B}_1 & -\mathcal{C}_1 & \cdots & 0 & 0 \\ -\mathcal{A}_1 & \mathcal{B}_2 & \cdots & 0 & 0 \\ 0 & -\mathcal{A}_2 & \cdots & 0 & 0 \\ \vdots & \vdots & \ddots & \vdots & \vdots \\ 0 & 0 & \cdots & \mathcal{B}_{N-1} & -\mathcal{C}_{N-1} \\ 0 & 0 & \cdots & -\mathcal{A}_{N-1} & \mathcal{B}_N \end{pmatrix} \cdot \begin{pmatrix} \boldsymbol{P}_1 \\ \boldsymbol{P}_2 \\ \boldsymbol{P}_3 \\ \vdots \\ \boldsymbol{P}_{N-1} \\ \boldsymbol{P}_N \end{pmatrix} = \begin{pmatrix} \boldsymbol{D}_1 \\ \boldsymbol{D}_2 \\ \boldsymbol{D}_3 \\ \vdots \\ \boldsymbol{D}_{N-1} \\ \boldsymbol{D}_N \end{pmatrix}$$

where $\mathcal{A}_i$, $\mathcal{B}_i$ and $\mathcal{C}_i$ are 4x4 matrices, and $\boldsymbol{D}_i$ and $\boldsymbol{P}_i$ are 4 element vectors. The first and the last row are derived from the boundary conditions:

$$\begin{aligned} \mathcal{B}_1 &= \Delta_1/\delta_1 + \mathbb{1}/\delta_1 + \mathcal{K}_1 \\ \mathcal{C}_1 &= \Delta_1/\delta_1 \\ \boldsymbol{D}_1 &= \frac{1}{2}\boldsymbol{J}_1 \\ \mathcal{A}_N &= \Delta_{N-1} - \frac{1}{2}\mathbb{1} \\ \mathcal{B}_N &= \Delta_{N-1} + \frac{1}{2}\mathbb{1} \\ \boldsymbol{D}_N &= \frac{1}{2}\left(\mathrm{B}_{\lambda N} + \mathrm{B}_{\lambda N-1}\right)\boldsymbol{e}_0 + \\ &\quad \Delta_{N-1}\left(\mathrm{B}_{\lambda N} - \mathrm{B}_{\lambda N-1}\right)\boldsymbol{e}_0 \end{aligned} \tag{26}$$

while the second-order equation couples 3 diagonals:

$$\begin{aligned} \mathcal{A}_i &= 2\Delta_{i-1}/(\delta_i + \delta_{i-1}) \\ \mathcal{B}_i &= 2\Delta_{i-1}/(\delta_i + \delta_{i-1}) + 2\Delta_i/(\delta_i + \delta_{i-1}) + \mathcal{K}_i \\ \mathcal{C}_i &= 2\Delta_i/(\delta_i + \delta_{i-1}). \end{aligned} \tag{27}$$

We note that the whole set of equations (26) and (27) is a block tri-diagonal linear system that can be solved with the conventional forward and backward elimination procedure. First, we get rid of the lower diagonal elements ($\mathcal{A}$'s) and bring diagonal matrices $\mathcal{B}$'s to $\mathbb{1}$:

$$\begin{aligned} \mathcal{C}'_1 &= \mathcal{B}_1^{-1}\mathcal{C}_1 \\ \mathcal{C}'_i &= \left(\mathcal{B}_i - \mathcal{A}_{i-1}\mathcal{C}'_{i-1}\right)^{-1}\mathcal{C}_i \\ \boldsymbol{D}'_1 &= \mathcal{B}_1^{-1}\boldsymbol{D}_1 \\ \boldsymbol{D}'_i &= \left(\mathcal{B}_i - \mathcal{A}_{i-1}\mathcal{C}'_{i-1}\right)^{-1}\left(\boldsymbol{D}_i + \mathcal{A}_{i-1}\boldsymbol{D}'_{i-1}\right), \end{aligned} \tag{28}$$

where $\mathcal{C}'$ is the new upper diagonal and $\boldsymbol{D}'$ is the new right-hand side. Next we perform the back substitution to obtain vectors $\boldsymbol{P}$:

$$\begin{aligned} \boldsymbol{P}_N &= \boldsymbol{D}'_N \\ \boldsymbol{P}_i &= \boldsymbol{D}'_i + \mathcal{C}'_i\boldsymbol{P}_{i+1}. \end{aligned} \tag{29}$$

The emerging Stokes vector $\boldsymbol{I}|_{z=0} = \boldsymbol{I}^+|_{z=0} = 2\boldsymbol{P}_1$

The method is fast and efficient as in the non-magnetic case but suffers from numerical instability in the case of strong lines and substantial field. Indeed, the forward substitution evaluates the new upper diagonal $\mathcal{C}'$ and the new right-hand side $\boldsymbol{D}'$ by computing the inverse of two matrices $\mathcal{B}_1$ and $\mathcal{B}_i - \mathcal{A}_{i-1}\mathcal{C}'_{i-1}$. The latter may lead to numerical instability that can be illustrated by the following example. Let us consider the situation where the direction of the field is parallel to the line of sight, the wavelength nearly coincides with the center of one of the σ-components (for example, red shifted) and the field is strong enough so that the contributions of other components in a given wavelength are small. We also assume the line to be strong and ignore the continuum opacity. Several components of the absorption matrix will vanish due to our assumptions ($\sin\gamma = 0$, $\phi_b \approx 0$ and $\phi_p \approx 0$):

$$\begin{aligned} \phi_I &= 1/2(\phi_p \sin^2\gamma + \\ &\quad 1/2(\phi_r + \phi_b)(1 + \cos^2\gamma)) + \alpha_{\mathrm{cont}} && \approx 1/2\phi_r \\ \phi_Q &= 1/2(\phi_p - 1/2(\phi_r + \phi_b))\sin^2\gamma\cos 2\chi && = 0 \\ \phi_U &= 1/2(\phi_p - 1/2(\phi_r + \phi_b))\sin^2\gamma\sin 2\chi && = 0 \\ \phi_V &= 1/2(\phi_r - \phi_b)\cos\gamma && \approx 1/2\phi_r \\ \psi_Q &= 1/2(\psi_p - 1/2(\psi_r + \psi_b))\sin^2\gamma\cos 2\chi && = 0 \\ \psi_U &= 1/2(\psi_p - 1/2(\psi_r + \psi_b))\sin^2\gamma\sin 2\chi && = 0 \\ \psi_V &= 1/2(\psi_r - \psi_b)\cos\gamma && \approx 1/2\psi_r, \end{aligned}$$

and the absorption matrix itself will be reduced to:

$$\mathcal{K} \approx \begin{pmatrix} 1/2\phi_r & 0 & 0 & 1/2\phi_r \\ 0 & 1/2\phi_r & 1/2\psi_r & 0 \\ 0 & -1/2\psi_r & 1/2\phi_r & 0 \\ 1/2\phi_r & 0 & 0 & 1/2\phi_r \end{pmatrix}$$

with ψ_r quite small because the Faraday-Voigt function for σ_r-component is very close to zero. The inverse of the absorption matrix required to evaluate Δ_i (eq. 25) is not well-conditioned and so will be the derived matrices. The result of such instability is illustrated in Figure 2. One should note that instead of evaluating the inverse matrices in equation (28) we can solve the system of linear equations with the matrix $\mathcal{B}_i - \mathcal{A}_{i-1}\mathcal{C}'_{i-1}$ and the right-hand sides $\mathcal{C}_i$ and $(\boldsymbol{D}_i + \mathcal{A}_{i-1}\boldsymbol{D}'_{i-1})$.

This is both more robust and more efficient: for example, using the LU decomposition algorithm (e.g. Press et al., 1986), one can decompose the matrix only once and then use it for all 5 columns of the right-hand sides.

The Feautrier method is very useful in the case where we are interested to know the radiation field throughout the whole atmosphere. Spectral synthesis of polarized radiation in INVERS10 only requires the knowledge of the emergent Stokes parameters, therefore we also considered the short characteristics DELO method.

2.2. DELO RTS

The Diagonal Element Lambda Iteration method has been suggested by Rees et al. (1989) who noted that the absorption matrix $\mathcal{K}$ is dominated by the main diagonal elements which are identical for each spectral line. Let us consider a case of an isolated line. In this

case the diagonal elements of $\mathcal{K}$ given by equation (5) are $k_c + k_0^{\rm line}\phi_I$ Introducing a modified absorption matrix and emission vector:

$$\mathcal{K}' = \mathcal{K}/k^{\rm tot} - \mathbb{1} \quad (30)$$

$$S' = J/k^{\rm tot}, \quad (31)$$

where $k^{\rm tot} = k_c + k_0^{\rm line}\phi_I$ and the optical depth as $d\tau = -k^{\rm tot}dz$ we can re-write the radiative transfer equation in the form:

$$\frac{dI}{d\tau} = I - (S' - \mathcal{K}'I) = I - S. \quad (32)$$

The new source function vector $S = (S' - \mathcal{K}'I)$ is not my different from S' because $\mathcal{K}'$ is small. For a given depth interval between points τ_i and τ_{i+1} the formal solution of equation (32) can be written as:

$$I(\tau_i) = \epsilon_i I(\tau_{i+1}) + \int_{\tau_i}^{\tau_{i+1}} e^{-(\tau-\tau_i)}S(\tau)d\tau, \quad (33)$$

where:

$$\epsilon_i = e^{-\delta_i} \text{ and } \delta_i = \tau_{i+1} - \tau_i. \quad (34)$$

Equation (33) looks like a standard radiative transfer equation written in an integral form (*S* depends on the Stokes vector), but noting that $\mathcal{K}'I$ is small, Rees et al. (1989) approximate $S(\tau)$ with a linear function:

$$S(\tau) = [(\tau_{i+1} - \tau)S_i + (\tau - \tau_i)S_{i+1}]/\delta_i, \quad (35)$$

and substituting this expression into equation (33) we can take the integral ***analytically*** (see equations (62)-(67) in Rees et al., 1989). This gives us a linear relation between Stokes vectors in ***i*** + 1 and ***i:***

$$I(\tau_i) = \mathcal{X}_i + \mathcal{Y}_i I(\tau_{i+1}), \quad (36)$$

where:

$$\begin{aligned} \mathcal{X}_i &= [\mathbb{1} + (\alpha_i - \beta_i)\mathcal{K}_i']^{-1} \cdot \\ &\quad [(\alpha_i - \beta_i)S_i' + \beta_i S_{i+1}'] \\ \mathcal{Y}_i &= [\mathbb{1} + (\alpha_i - \beta_i)\mathcal{K}_i']^{-1} \cdot (\epsilon_i \mathbb{1} - \beta_i \mathcal{K}_{i+1}') \\ \alpha_i &= 1 - \epsilon_i \\ \beta_i &= [1 - (1 + \delta_i)\epsilon_i]/\delta_i. \end{aligned} \quad (37)$$

The boundary condition for equation (33) is set for deep layers in the atmosphere. The corresponding asymptotic approximation is readily given by equation (23). The main advantage of the DELO method is that it requires only one pass through the atmosphere because the Stokes vector in the current point is derived from the Stokes vector in the previous (deeper) point, the absorption matrix and the source function. The need to know the equation parameters only in two adjacent points makes DELO a short characteristics method. Equations (37) can be generalized to the case of multiple blended lines and column mass as a depth parameter. Before doing it, we note that in case of a blend the diagonal elements of $\mathcal{K}$ will be $k_c + \sum k_o^{\rm line}\phi_I^{\rm line}$, so the new definition for $k^{\rm tot}$ should be

$$k^{\rm tot} = k_c + \sum_{\rm lines} k_o^{\rm line}\phi_I^{\rm line}. \quad (38)$$

We also note that $\delta_i \approx {}^1/_2(k_i^{\rm tot} + k_{i+1}^{\rm tot})(m_{i+1} - m_i)$. The rest of the derivation of equations (36) and (37) holds directly. The integration starts from the deep layers where the initial Stokes vector is given by equation (23), then for each step we evaluate matrices $\mathcal{X}$ and $\mathcal{Y}$ using equations (37) and compute the next Stokes vector from equation (36). Note that only one matrix inversion is required for computing $\mathcal{X}$ and $\mathcal{Y}$ at each step, but this inversion is numerically stable because for small δ_i, $(\alpha_i - \beta_i)$ is of the order of $\delta_i/2$ and the matrix $\mathbb{1} + {}^1/_2\delta_i\mathcal{K}_i'$ is dominated by its main diagonal. The accuracy of the DELO method primarily depends on the accuracy of the linear approximation for S given by equation (35). One can reach high precision for the emerging Stokes vector by refining the depth grid so that for each interval i the difference between $S'(m_{i+1/2})$ and ${}^1/_2(S_i' + S_{i+1}')$ is small (we use S' as an approximation for *S*).

DELO is not quite a second-order method but it is fast, robust and sufficiently accurate to be used in INVERS10. Figures 3 and 4 show good agreement between spectra of two Stokes parameters computed with the two methods in the presence of magnetic field. The DELO algorithm was 30% faster than the Feautrier.

2.3. The quality of spectral synthesis

The methods of solving the radiative transfer equation described above have certain (quite high) numerical precision, but other effects may be significant or even dominating the quality of synthetic spectra. The two major players are the model atmosphere and the atomic data.

Model atmospheres in use today are mostly ID, plane-parallel, computed in LTE with a very primitive treatment of convection (mixing length theory) and uncertain opacity sources (e.g. autoionizing lines). We are forced to introduce two fudge parameters (micro- and macro-turbulence) to partially compensate for some of the assumptions. Recent attempts to compute 3D hydrodynamic models (Asplund et al., 1999) give very encouraging results, but such models are very costly and very sparse. Although the simplifications listed above may be very far from reality, the resulting temperature structure in the line forming regions is good enough for spectral synthesis. Even a simple LTE spectral synthesis code can do very well in the reproduction of the disk integrated monochromatic fluxes. Figure 5 shows the comparison of the NSO FTS Solar spectrum (Kurucz et al., 1984) with the LTE calculations performed with the **SYNTHMAG**

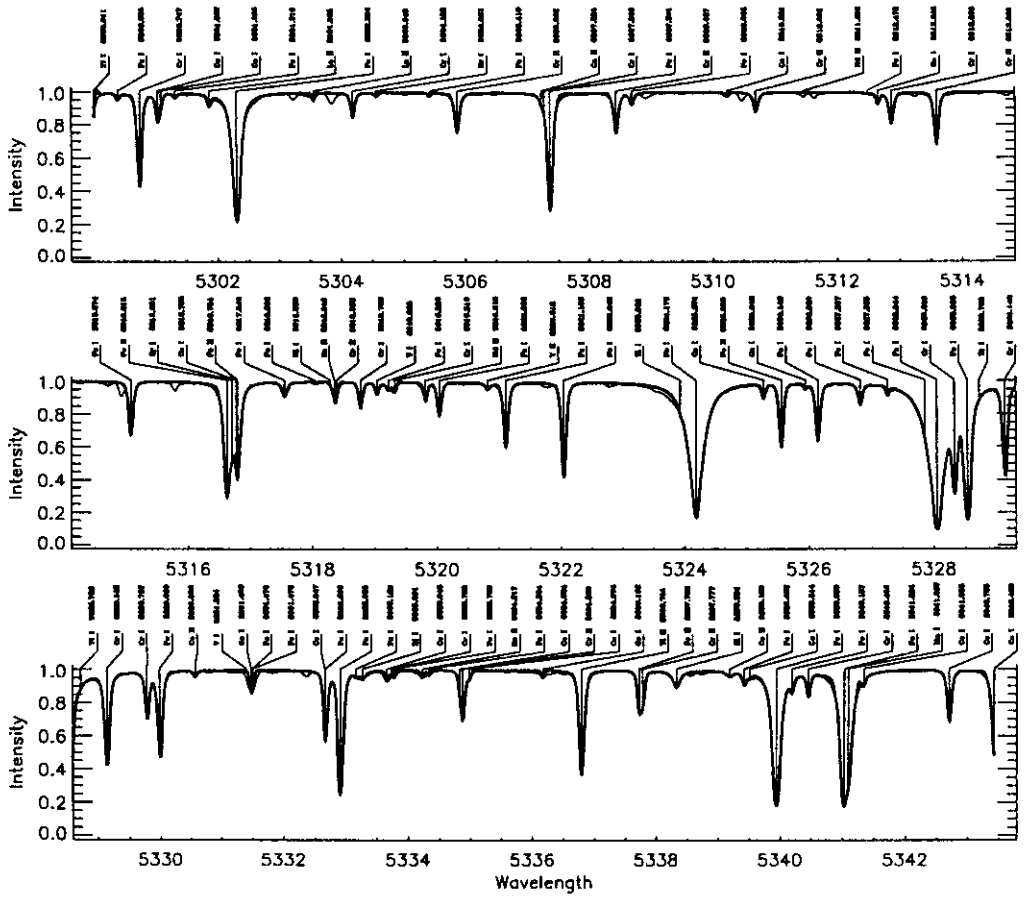

Figure 5: *The LTE synthesis of the solar spectrum using the theoretical model atmosphere (thick line) compared to the FTS full disk solar spectrum (thin line).*

code (Piskunov, 1999) based on the Feautrier RTS for the solar LTE model computed by Kurucz (1993). We conclude that ***the most significant deviations are due to the errors in the transition parameters or non-identified lines.*** The deficiency of the model can be seen for the best fitted lines as the systematic asymmetry of the profiles. Only a very tiny fraction of lines formed in the photosphere shows noticeable NLTE effects (Cal 6439 **A** is one good example). Such a comparison encouraged us to use the same approach to study fast rotating stars suitable for Doppler Imaging.

3. Solving the inverse problem for MDI

The inverse problem for Magnetic Doppler Imaging is similar to the conventional Doppler Imaging. We perform a conditional minimization of the discrepancy functional Ξ (Piskunov & Rice, 1993):

$$\Xi = \sum_{\phi,\lambda} \left[R_I(\phi,\lambda)^{\rm calc} - R_I(\phi,\lambda)^{\rm obs}\right]^2 \quad (39)$$

$$\Phi \equiv \Xi + \Omega = \min, \quad (40)$$

where ϕ and λ are the observed rotational phases and wavelengths and R_I are the disk integrated Stokes vectors. The regularization functional Ω is used to ensure a unique solution by restricting the space of possible solutions. It is fairly easy to compute the first derivatives of Ξ in respect to the local parameters (magnetic vector components and element abundance) as this can be done in the same loops as the calculation of $R_I(\phi,\lambda)^{\rm calc}$ themselves:

$$R_I = \sum_{surface} I_{\phi\lambda+\Delta\lambda_{\rm Dop}}(A,\vec{\rm B})\mu\Delta\sigma, \quad (41)$$

$$\Xi' = \sum_{\phi,\lambda} \left[R_I^{\rm calc} - R_I^{\rm obs}\right] I'_{\phi\lambda+\Delta\lambda_{\rm Dop}}(A,\vec{\rm B})\mu\Delta\sigma, \quad (42)$$

where $\mu\Delta\sigma$ is the projected area of the surface element. Note that the absence of integration over the surface for Ξ' reflects the fact that the derivative is taken with respect to the local element of the map. If we can compute I' simultaneously with I, it will take only a minor additional effort to evaluate Ξ' together with Ξ.

This property is very general for all inverse problems encountered in remote sensing and allows efficient parallelization of the computations (see the next section).

The large number of variables and the availability of the first derivatives motivates the use of the conjugate gradient minimization method (Press et al., **1986).** Theoretically, a number of iterations similar to the number of variables **(2000-4000)** is needed to reach the convergence with this method, but in practice we reach the level close to the accuracy of the observations already in $\approx$**100** iterations and we see no significant improvement after that due to systematic effects (missing or erroneous line data, data reduction problems etc.) Even **100** iterations require a very powerful computer. An alternative solution is to use Newton-type algorithms (e.g. Marquardt-Levenberg, **1994)** for the minimization of **(40).** These algorithms are much more efficient **(2nd**-order) in the vicinity of the solution. Our tests show that we can achieve convergence in **3-4** iterations effectively trading memory for speed (The Marquardt-Levenberg algorithm requires storing a matrix of size *Nsizeofmap* $\times$ *sizeof observations).*

4. Parallel execution

INVERS10 is designed for parallel execution. We used the Message Passing Interface (MPI) for organizing the interaction between processes. The initial concept was based on the fact that during each iteration spectral synthesis for each rotational phase can be performed independently. The current single-program-multiple-data implementation of **INVERS10** begins with reading in the observational data and the starting model and initialization of arrays that can be pre-computed. Next, the data is distributed between all processes by means of **MPI_BR0ADCAST** call. After that, each process takes approximately equal number of phases and computes spectral synthesis and derivatives of the local line profiles for the current distribution of magnetic field and abundance. It is useful to have the number of processes equal to the number of rotational phases. The main process collects computed spectra, corrects the maps and distributes them to all processes for the next iteration.

Although the code based on this concept performs well and scales almost linearly with the number of CPUs, it has two important limitations:

• no performance improvement is possible after the number of CPUs has reached the number of observed phases;

• load balance is difficult to achieve. Each iteration takes as long as the slowest process which does approximately as much work (phases) as the other faster processes.

An alternative MPI-based algorithm for parallel execution has been implemented in our non-magnetic DI code for multi-element abundance mapping **INVERS12.** (In this code we have also implemented the Marquardt-Levenberg algorithm mentioned in the previous section). The parallel scheme consists of the following steps:

1° Input data and initialize radiative transfer solvers (main process).

2° Start minimization (main process).

3° Compute local spectra and their derivatives:

4° Continue the minimization of Φ.

5° When the minimum is achieved, signal to the subordinate processes to exit.

During step 3° the ***main process:***

I Takes the next surface element and sends its abundances to the first available radiative transfer solver. Repeats this step (without waiting) until no free solver is available.

II Checks with MPI_WAITANY if any one of the solvers is ready.

III If one is found, retrieves I and I' and updates the disk integral.

IV If there are unprocessed surface elements left, passes the next one to this radiative transfer solver and goes back to II.

Meanwhile each ***subordinate process (radiative transfer solver):***

I Receives surface element (local abundances) from the main process.

II Solves the radiative transfer for all the wavelengths and all the phases to evaluate I, perturbs local abundances and computes I again to evaluate numerically the derivatives $\frac{\partial I}{\partial A}$

III Signals the completion to the main process.

IV Returns the results and waits for the next surface element.

We are working on implementing a similar scheme for **INVERS10.** Since the time spent on computing I ***for each surface element in each phase*** dominates the DI procedure, the advantages of such implementation are obvious:

• The total time for a single iteration is reduced proportionally to the number of available processors assigned to solve the radiative transfer. This will scale

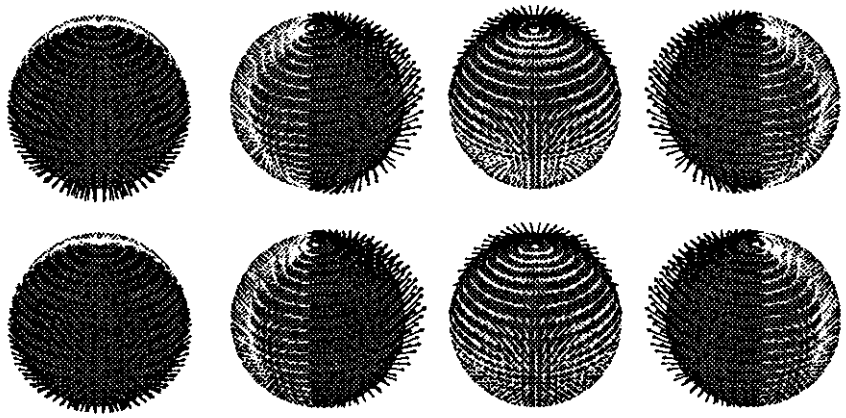

Figure 6: *The reconstruction of the dipolar field with the axis of the dipole inclined by 90° to the rotational axis. The inclination of the rotation axis i=60°. Kurucz model with* $T_{\rm eff} = 9000$ *K,* $\log g = 4$ *has been used for spectral synthesis of the 2 Fe* II *lines (6147.741 Å and 6149.258 Å). The inversion is based on four Stokes parameters. The original image is shown in the top panel and the reconstruction of the field vectors is presented in the lower panel. The black arrows show field vectors pointing outside the stellar surface while white arrows are pointing inside.*

linearly until the number of processors matches the number of surface elements **(2000-4000).**

• The CPU load is automatically balanced: faster radiative transfer solvers process more surface elements.

• Further speed increase can be achieved by taking advantage of the fact that some computationally expensive functions (e.g. Voigt and Faradey-Voigt) do not depend on the rotational phase (Zeeman splitting is proportional to the field strength and is not influenced by field orientation) so they have to be evaluated only at one phase for each surface element.

• Local memory per process has (modest) dimensions of the observed data set.

5. Numerical experiments

At this time we do not have any complete set of polarization observations in **4** Stokes parameters with adequate quality for applying **INVERS10.** In fact, only **2-3** stellar telescopes in the world have high resolution spectrometers equipped with analyzers capable of registering **4** Stokes parameters. In preparation for the real data we have been studying **INVERS10** using numerical calculations. For a given magnetic field configuration we are computing the fake observational data with a given spectral resolution and S/N ratio. The simulated data are produced using a variety of grids and sometimes a different algorithm (e.g. SYNTHMAG). Then we run the inversion and compare the results with the original map.

Our extensive program of testing the performance of **INVERS10** is described by Kochukhov (this proceedings). Here we just give **2** examples. Figure **6** shows the reconstruction of a simple dipolar field based on simulated **4** Stokes parameter data. The reconstruction is nearly perfect in the northern hemisphere. We were surprised by the ability of our MDI code to recover the correct field configuration even for very slow rotators ($v\sin i < 15$km s^{-1}). This reflects the influence of the field vector orientation on the observed polarization spectra.

Figure **7** is demonstrating the ability of reconstructing the radial field concentrated in a small "active" region.

6. Conclusions

We have developed a new MDI code **INVERS10** capable of simultaneously reconstructing the distribution of magnetic field vectors and abundance of one chemical element on the surface of a CP star. The code solves the radiative transfer for **4** Stokes parameters "on the fly" with a state-of-the-art DELO algorithm and uses the MPI environment for parallel computing. Extensive numerical experiments and comparisons with other magnetic spectral synthesis codes and with the solar atlas confirmed the high accuracy and high speed of the new program and demonstrate its ability to reconstruct a variety of field geometries from simple dipolar to a superposition of several multipoles with and without abundance spots. We also confirmed the necessity to use spectra in all **4** Stokes parameters in order to ensure the uniqueness of the solution. We intend to use **INVERS10** to interprete such data sets as they will become available. We

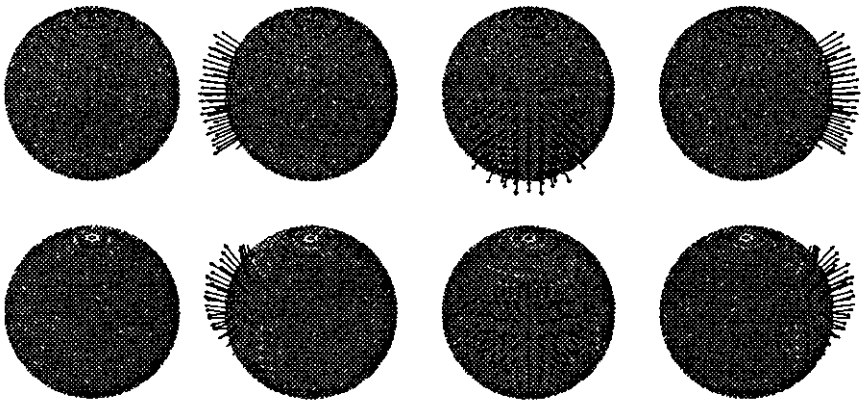

Figure 7: *The reconstruction of the radial field concentrated in a circular spot on stellar equator. The parameters of the model star and spectral interval are the same as in Fig. 6. The original image is shown in the top panel and the reconstruction of the field vectors is presented in the lower panel.*

also plan to adapt the new program for imaging active late-type stars with complex field structures. We will still work on the structure of the new code implementing new parallelization techniques and a more efficient minimization algorithm tested already in another DI code.

Among new features revealed during numerical experiments we discovered the ability of INVERS10 to image magnetic fields on very slow rotating stars, unreachable for conventional DI technique.

Acknowledgements. We are grateful to the NSO/Kitt Peak for making the solar FTS data available. We acknowledge the Swedish Naturvetenskapliga Forskningsradet for the financial support and the Knut & Alice Wallenberg Foundation for granting the supercomputer facility at Uppsala Observatory that was extensively used in this work. We also thank the Swedish Royal Academy of Sciences for supporting our collaboration with the Russian Special Astrophysical Observatory.

References

Averbukh V.Z., Figueroa S., Schlick T., 1994, ACM Trans. Math. Softw., 20, 282

Allard F., and Hauschildt P. H., 1995, Astrophys, J., 445, 433

Asplund M., 1999, in: Proceedings of the 11th Cambridge Workshop on Cool Stars, Stellar Systems, and the Sun, R.J. Garcia Lopez, R. Rebolo and M.R. Zapatero Osorio (eds.), Puerto de la Cruz, Tenerife 1999, ASP, San Francisco, in press

Auer L.H., Heasley J.N., and House L.L., 1977, Astrophys. J., 216, 531

Deutsch A., 1958, Electromagnetic Phenomena in Cosmical Physics, IAU Symp. No. 6, ed. B. Lehnert, Stockholm 1956, Cambridge Univ. Press, 209

Goncharsky A.V., Stepanov V.V., Khokhlova V.L., Yagola A.G., 1982, Astron. Zh., 59, 1146

Humlic'ek J., 1982, JQSRT, 27, 437

Kurucz R.L., 1993 CD-ROM, No.13

Kurucz R.L., Furenlid I., Brault J., and Testerman L., 1984, N.S.O. Atlas, No.1

Landi DegI'Innocenti E., 1976, Astron. Astrophys. Suppl. Ser., 25, 379

Piskunov N., 1999, in: Proceedings of the 2nd Workshop on Solar Polarization, J. Stenflo and K.N. Nagendra (eds.), 1998, Bangalore, India, Kluwer, 515

Piskunov N. 1998, in: Proceedings of the 10th Cambridge Workshop on Cool Stars, Stellar Systems, and the Sun, R.A. Donahue and J.A. Bookbinder (eds.), Cambridge MA 1997, ASP, San Francisco, CD-2029

Piskunov N., 1996, in: Proceedings of the 5th Vienna Workshop on Model Atmospheres and Spectral Synthesis, S.J. Adelman, F. Kupka and W.W. Weiss (eds.), Vienna 1995, ASP, San Francisco, 243

Piskunov N. and Rice J.B., 1993, Publ. Astr. Soc. Pacific, 105, No. 694, 1415

Piskunov N., Kupka F., Ryabchikova T.A., Weiss W.W., Jeffery C.S., 1995, Astron. Astrophys. Suppl. Ser., 112, 525

Piskunov N., 1992, in: Proceedings of the International meeting "Stellar Magnetism", Special Astrophys. Observatory, Nizhnij Arkhyz, 1991, eds.: Yu.V. Glagolevskij, I.I Romanuk, Nauka, St.Petersburg, 92

Press W. H., Flannery B. P., Teukolsky S. A., Vetterling W. T., 1986, Numerical Recipes, Cambridge University Press, Cambridge

Rees D.E., Murphy G.A. and Durrant C.J., 1989, Astrophys. J., 339, 1093

Johns-Krull CM. and Valenti J.A., 1996, Astrophys. J. Lett., 459, L95

Valenti J.A. and Piskunov N., 1996, Astron. Astrophys., 118, 595

Valenti J.A, Piskunov N., Johns-Krull CM., 1998, Astrophys. J., 498, 851